

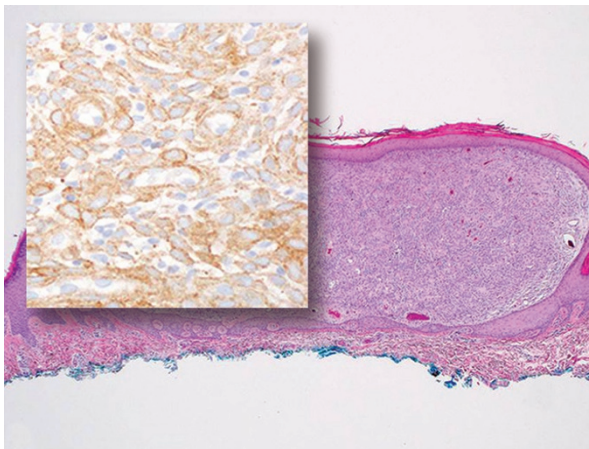
INSIDE THE USCAP JOURNALS

doi:10.1038/modpathol.2015.73

MODERN PATHOLOGY

ALK rearrangement in epithelioid fibrous histiocytoma

See page 904

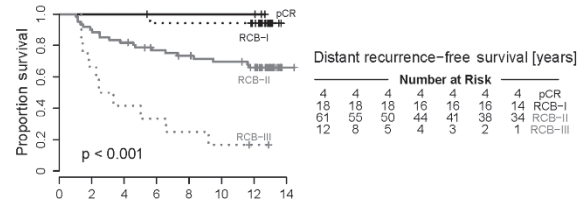


The pace of discovery of recurrent gene fusions has been augmented by the application of next-generation sequencing techniques. Based on prior case reports of epithelioid fibrous histiocytomas with *ALK* rearrangements, Doyle *et al* examined both *ALK* expression by immunohistochemistry and *ALK* rearrangement by fluorescence *in situ* hybridization (FISH) in 33 cases of epithelioid fibrous histiocytoma. Fully 88% showed *ALK* expression, and all 13 cases examined by FISH showed *ALK* rearrangement. Two prior cases examined by next-generation sequencing showed *VCL* and *SQSTM1* as *ALK* fusion partners. As with other *ALK* translocated neoplasms, there may be a wide range of partners. *ALK* expression may have diagnostic utility as *ALK* was not seen in an appropriate series of potential histologic mimics. This study distinguishes epithelioid fibrous histiocytomas from classic fibrous histiocytomas (dermatofibromas), a subset of which harbor *PRKCB* and *PRKCD* fusions with multiple genes leading to increased protein kinase C activity

Residual breast cancer burden assessment is reproducible

See page 913

The residual breast cancer burden (RCB) index quantifies residual disease following neoadjuvant chemotherapy. The scale ranges from pathologic complete response to extensive residual disease and is robust prognostic indicator. Peintinger and colleagues used this index to assess, via slides and pathology reports, 100 cases in patients treated in a randomized neoadjuvant trial

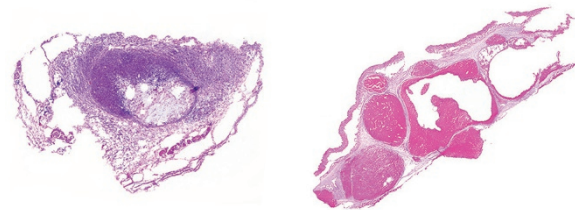


with a median follow-up of 12 years. Pathologists from five centers reviewed the cases to determine levels of reproducibility. The overall concordance correlation coefficient for agreement in RCB score was high: 0.931, with accuracy of 0.989. Overall concordance was superior for metastatic disease than for primary tumors. In addition to the relatively small differences between the five pathologists' scores, each individual's scores had essentially the same prognostic accuracy for both distant recurrence-free survival and overall survival (overall concordance correlation coefficient: 0.995). The robust predictive nature of the RCB index was previously well documented, but this study shows that the assessments are highly reproducible as well.

LABORATORY INVESTIGATION

Insights from an infantile hemangioma model

See page 765

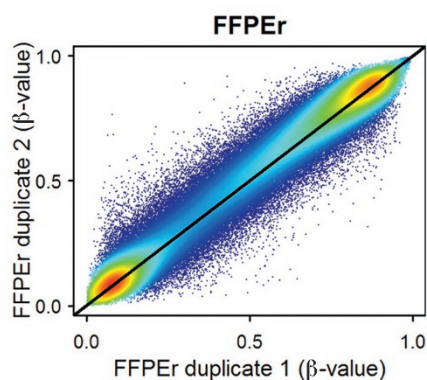


Infantile hemangiomas are common benign tumors that usually involute and resolve, but they can be associated with scarring. Tsuneki and colleagues implanted microvascular endothelial cells in three-dimensional hydrogel scaffolds into mice to form microvessel networks. Over time, these integrated with host vessels and remodeled into large ectatic vascular structures resembling hemangiomas. Additional observation detected proliferative and involutinal phases similar to those of infantile hemangiomas. As with human infantile hemangiomas, the proliferative phase was peppered with lymphocytes and other mononuclear cells that were greatly reduced during involution. Involution was characterized by a loss of the Hippo pathway components *Ajuba* and *YAP* along with *Survivin*, as seen in immunohistochemistry results similar to those of

human biopsies. This model suggests that there is an immunologic component of the proliferative phase and that involution might be induced by treatment with currently available inhibitors of Survivin and Ajuba.

Assessment of genomic methylation using FFPE tissue samples

See page 833



A cell's genomic methylation state—a critical determinant of differentiation—helps to maintain differences between cell types and tissues that have identical genomic sequences. Methylation influences chromatin structure and gene expression in normal and neoplastic processes. Clinical assessment of individual genes for methylation is performed using formalin-fixed, paraffin-embedded (FFPE) material, for example, in examination of promoter methylation of *MLH1* to determine whether microsatellite-unstable colonic carcinoma is due to a somatic or germ-line event. However, the material available for global assessment of genomic methylation patterns has been limited to fresh-frozen tissue. de Ruijter *et al* now show that this can be done with FFPE material as well. Using as little as 100 ng of DNA and a DNA-restoration procedure, they showed high correlation of FFPE results with those from cognate fresh-frozen tissue. The results were confirmed using methylation-specific PCR. Examination of genomic methylation is now applicable to FFPE archives.

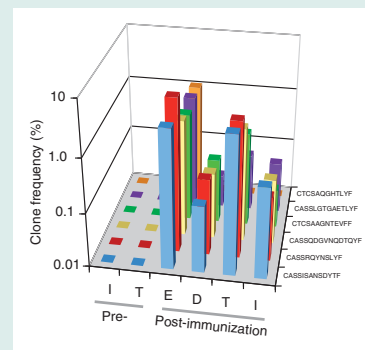
MODERN PATHOLOGY (2015) 28, 882–883

nature.com/pathology

Common clonal origins for T cells with skin immunization

Lymph nodes harbor central memory T (TCM) cells, whereas resident memory T (TRM) cells are by definition in peripheral tissue. Both types of cells are generated after primary infections, but they have distinct roles in protective immunity. In a study reported in *Nature Medicine*, Gaide *et al* explored the clonal origins of these two groups by immunizing mouse skin with various antigens and analyzing antigen-activated T cells from different tissues for clonality, using next-generation sequencing to produce CDR3 sequences. When abundant TRM cell clones are generated in the skin, identical clones are detectable in the TCM fraction of the lymph node. Both the TRM and TCM populations with overlapping TCR repertoires were derived from a common naive T-cell precursor as a result of immunization. The TCM cells mediated delayed and attenuated responses, and the TRM cells mediated rapid contact hypersensitivity. Portions of these studies were confirmed in humans with allergic contact dermatitis.

Nature Medicine, published online 11 May 2015; doi:10.1038/nm.3860



A better understanding of osteosarcoma

Osteosarcoma is a genetically complex disease with a strong propensity to metastasize to the lung. Its significant genetic complexity has complicated the search for driver genes in the genomic characterizations performed to date. As reported in *Nature Genetics*, Moriarity *et al* used a *Sleeping Beauty* forward genetic screen to discover genes involved in osteosarcoma genesis and metastatic progression in mice with and without somatic loss of *Trp53*. Using this method, they identified 232 sites potentially associated with osteosarcoma development and another 43 sites associated with metastasis. The implicated genes were enriched in the ErbB, PI3K-AKT-mTOR, and ERK pathways commonly seen in many cancers. *Nf1* loss, which was common, corresponds to reports in humans of an increased incidence of osteosarcoma in the setting of neurofibromatosis type 1. Two genes involved in neuronal axon guidance, *Sema4d* and *Sema6d*, were also identified and confirmed as novel oncogenes in human osteosarcoma.

Nature Genetics 2015;47:615–624; doi:10.1038/ng.3293

Human tissue-specific networks

The specific properties of cells and tissues are critical factors underlying both human physiology and disease. We lack a complete understanding of the genetic basis of tissues and cell lineages. As described in *Nature Genetics*, Greene *et al* addressed this gap by integrating genetic data sets from more than 14,000 distinct publications. Using approaches that can extract both functional and tissue-specific signals, they mapped patterns of protein interactions based on genetic data. Rather than assuming that a pathway has the same function and consequences regardless of the type of cells in which it occurs, this approach allowed exploration of the function of pathways and protein in 144 tissue- and cell-lineage-specific contexts. The authors have developed a tool, called NetWAS, that, by incorporating cellular context, more accurately maps genes to disease in comparison to genome-wide associations study alone. In addition, their website, GIANT, is a resource for exploring potential network interactions across many cell types.

Nature Genetics 2015;47:569–576; doi:10.1038/ng.3259

